Optimal Design of High-Frequency Magnetic-Links for Power Converters Used in Grid Connected Renewable Energy Systems

Md. Rabiul Islam, Gang Lei, Youguang Guo, *Senior Member, IEEE*, and Jianguo Zhu, *Senior Member*, *IEEE*

University of Technology Sydney, P. O. Box 123, Broadway, NSW 2007, Australia

Recently the high-frequency common magnetic-links instead of common dc-links with advanced magnetic materials, such as nanocrystalline and amorphous materials have been considered as viable candidates for the development of medium-voltage power converters. This offers a new route of step-up-transformer-less compact and lightweight direct grid integration of renewable generation systems. Most importantly, it minimizes the voltage imbalance and common mode issues of the converter systems. However, the electromagnetic design of the high-frequency common magnetic-links is a multi-physics problem and thereby affects the system efficiency and cost. In this paper, an optimization technique is proposed and verified with the prototype magnetic-links. The design and optimization, implementation, test platform, and the experimental test results are analyzed and discussed.

Index Terms— **Design optimization, high-frequency magnetic-links, nanocrystalline and amorphous materials, smart grid**

I. INTRODUCTION

WITH THE RAPID growth of renewable power generation, the development of medium-voltage converters for step-up-transformer-less direct grid connection of renewable power generation systems has attracted significant attention in the recent years [1], [2]. Due to the common/multiple dc-links and direct grid connection, the present technologies have some critical limitations, such as voltage imbalance, limited maximum power extraction, and common-mode problems. As an alternative approach, a common magnetic-link (instead of common/multiple dc-link) was proposed to eliminate most of the above limitations [3]. Fe-based amorphous and nanocrystalline alloys have attracted a high degree of attention because of their significantly low magnetic core losses and very high magnetic flux density [4]–[8]. Due to their superior performance Fe-based amorphous ribbons have been used in high power applications [9], [10]. Recently, a medium-voltage converter using amorphous alloy-based high-frequency common magnetic-link was validated and reported with adequate results, such as inherently voltage balancing and grid isolation and minimizing the limitation of maximum power extraction [11]. However, the design process of high-frequency magnetic-link involves multi-physics problems with some critical decision making tasks and thereby affects the power converter efficiency and cost. This paper proposes an optimal design process of high-frequency magnetic-links with advanced soft magnetic materials, e.g. amorphous alloys. The design and optimization, implementation, test platform, and the experimental test results are analyzed and discussed.

II. CORE MATERIAL SELECTION

The amorphous alloy and nanocrystalline magnetic materials have excellent magnetic properties, such as high permeability, high saturation flux density, and relatively low core losses. Two commercially available amorphous and nanocrystalline materials are Metglas and Finemet, which are

manufactured by Hitachi Metals, Japan. Although Finemet has lower specific core loss than Metglas, its saturation flux density (about 1 T) is much lower than that of Metglas (up to 1.56 T). The Metglas magnetic alloys 2705M and 2714A are cobalt-based materials with saturation inductions of 0.77 T and 0.57 T, and the specific core losses are about 6 W/kg and 3 W/kg, respectively, at 10 kHz sinusoidal excitation of 0.3 T. The alloy 2826MB is an iron nickel-based material with saturation flux density of 0.88 T and specific core loss of 30 W/kg at 10 kHz sinusoidal excitation of 0.3 T. The Metglas alloys 2605SA1 and 2605S3A are iron-based material with saturation flux density of 1.56 T and 1.41 T, and the specific core losses of 20 W/kg and 7 W/kg, respectively, at 10 kHz sinusoidal excitation of 0.3 T. Taking into account the flux density, specific core loss, and cost, Metglas alloys 2605S3A and 2605SA1 can be excellent choices for large capacity high-frequency transformers. Table I tabulates the properties of Metglas alloys 2605S3A and 2605SA1. The specific core loss under sinusoidal voltage excitation can be modelled by the Steinmetz law

$$P_{core} = kf^m B^n \tag{1}$$

where the coefficients k, m and n can be derived from the core losses provided in the datasheet, f is the frequency in kHz and B the magnitude of flux density in T.

Usually the high-frequency magnetic-links are operated with non-sinusoidal voltage excitation. Therefore, for this design new coefficients are calculated by measurements under square voltage excitation. The newly derived coefficients are summarized in Table II. Fig. 1 shows the calculated core losses of Metglas alloys 2605S3A and 2605SA1 with square-wave high-frequency excitation.

III. DESIGN AND OPTIMIZATION

The magnitude of average flux density over the cross section of the magnetic-link can be calculated by

$$B = \frac{V_{rms}}{4fNA} \tag{2}$$

where f is the excitation frequency, V_{rms} the winding voltage, A the cross sectional area of the transformer core, and N the number of turns of a winding. From the specifications of the magnetic-links and data sheets of the core materials, the magnetic-link initial parameters can be calculated. These parameters are used as the initial values of the optimization process. For structural simplicity, a toroidal core is considered.

TABLE I
PROPERTIES OF 2605S3A AND 2605SA1

Metglas alloys	2605S3A	2605SA1
Impedance permeability	0.0207, 0.0199, 0.0196 H/m at 1, 6, 10 kHz	0.0326, 0.0188, 0.0138 H/m at 1, 6, 10 kHz
Resistivity	138 μΩcm	130 μΩcm
Curie temperature	358 ºC	395 ºC
Magnetostriction	20 ppm	27 ppm
Mass density	7.29 g/cm³	7.18 g/cm³

TABLE II
COEFFICIENTS OF STEINMETZ EQUATION WITH SQUARE-WAVE HIGH-FREQUENCY EXCITATION

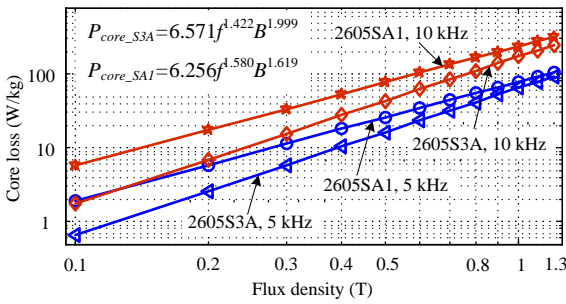| Core material	Coefficients		
	k	m	n
2605S3A	6.571	1.422	1.999
2605SA1	6.256	1.580	1.619

Fig. 1. Calculated core losses of Metglas alloys 2605S3A and 2605SA1 in terms of flux density and frequency with square-wave excitation.

In this paper, differential evolution algorithm (DEA) is used as the optimization algorithm. DEA was first presented in 1997 as a population based stochastic global optimization method [12]. Up to now, many studies have demonstrated that it converges fast is robust and simple to implement, and requires only a few control parameters. It has been widely employed for optimization of electromagnetic devices and has achieved many improvements [13], [14].

The procedure of DEA very similar to that of the genetic algorithm consists of three processes, namely mutation, crossover and selection. It starts by initializing the population randomly in the design space. The individuals in the population are then perturbed with others through mutation and crossover operators, and a new population consisting of the most promising solution can be generated by applying a selection criterion [12], [13].

In the implementation, the algorithm parameters of DEA are mutation factor of 0.8, crossover factor of 0.8, the maximum number of iteration of 1000, and the maximum stall generation of 100 (as the stop criterion) [14].

Different factors are considered during the optimization, such as the winding dimensions, hole reserve for natural cooling, maximum temperature limits, maximum power loss, availability of core material stripe dimensions (available sizes of alloys 2605S3A and 2605SA1: widths of 2.5–50 mm and 5–213 mm, respectively, and thickness of 20 μm), parasitic parameters, skin and proximity effects, and possibility to induce identical voltage in multiple secondary windings. In a conductor, the ac/dc resistance ratios depend strongly on the number of layers, the conductor diameter, and frequency. At high frequencies, associated with a small skin depth and proximity effect, the number of layers as well as the conductor diameter should be kept as small as possible. Moreover, the insulated strands should be twisted or braided together to equalize the flux linkages throughout the conductors. To achieve this and so as to reduce the winding loss, a Litz wire with small number of layers should be always used in a high-frequency magnetic-link. If R_{dc} is the dc resistance of a winding carrying a current of I, the skin effect loss in a Litz winding can be calculated from [15]

$$P_{skin} = I^2 R_{dc} \frac{\gamma}{4} \frac{ber(\gamma)bei'(\gamma) - bei(\gamma)ber'(\gamma)}{ber'(\gamma)^2 + bei'(\gamma)^2} \qquad (3)$$

where

$$\gamma = \frac{d}{2}\sqrt{\frac{\pi\mu f}{\rho}} \qquad (4)$$

and ber and bei are the real and imaginary parts of Bessel functions of the first kind and μ is the permeability of the core material, ρ the resistivity, and f the excitation frequency. Proximity effects can be classified into two types, the internal proximity effects: the effects on each of the strands due to the field generated by the strands, and the external proximity effects: the effects on an isolated round conductor within an external field. The power losses due to the internal and external proximity effects can be calculated by [15]

$$P_{in} = -\frac{\gamma n_s I^2 l_s}{4\pi\sigma r_b^2} \frac{ber_2(\gamma)ber'(\gamma) + bei_2(\gamma)bei'(\gamma)}{ber'(\gamma)^2 + bei'(\gamma)^2}. \qquad (5)$$

and

$$P_{ex} = -n_s H_e^2 \frac{2\pi\gamma}{\sigma} \frac{ber_2(\gamma)ber'(\gamma) + bei_2(\gamma)bei'(\gamma)}{ber'(\gamma)^2 + bei'(\gamma)^2}. \qquad (6)$$

where l_s is the total length of a single strand, n_s the total number of strands, r_b the radius of the bundle, σ the conductivity, and H_e the strength of the external magnetic field.

Taking into account the operating frequency of commercially available power semiconductor devices, a frequency window in the range of 1–20 kHz is considered in the optimization. The optimal parameters of 2.5 kVA magnetic links are summarized in Table III. The designs show that magnetic alloy 2605S3A has a slightly larger volume and weight but much lower specific core loss than that of alloy 2605SA1, and is suitable for high-frequency magnetic-links.

In the ANSOFT environment, two magnetic cores are modeled using the parameters obtained from optimization and non-sinusoidal high-frequency characteristics of Metglas alloys 2605S3A and 2605SA1. Fig. 2 shows the magnetic field distribution of Metglas alloy 2605S3A with square wave voltage excitation at 6 kHz. Fig. 3 shows the magnetic field distribution of Metglas alloy 2605SA1. Figs 2 and 3 show the transient magnetic fields caused by the time-varying electrical source. Therefore, field distributions appeared in these figures for particular times are inhomogeneous and asymmetric.

TABLE III
OPTIMAL PARAMETERS FOR 2.5 kVA MAGNETIC-LINKS

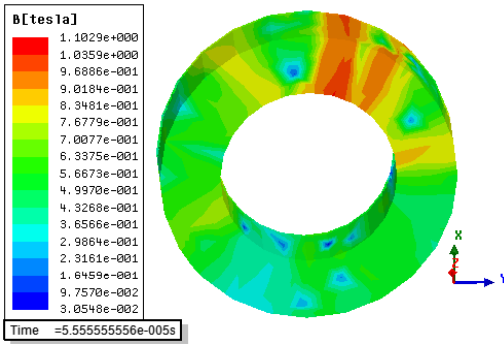| Core material	Parameters						
	WD (cm)	HT (cm)	B (T)	f (kHz)	Vol. (cm^3)	Wt. (kg)	P_{core} (W/kg)
2605S3A	2.22	2.78	1	6.05	169	1.23	71
2605SA1	2.29	2.61	1	6.25	165	1.18	96

Fig. 2. Magnetic field illustration for Metglas alloy 2605S3A-based high-frequency magnetic-link in the ANSOFT (transient magnetic fields).
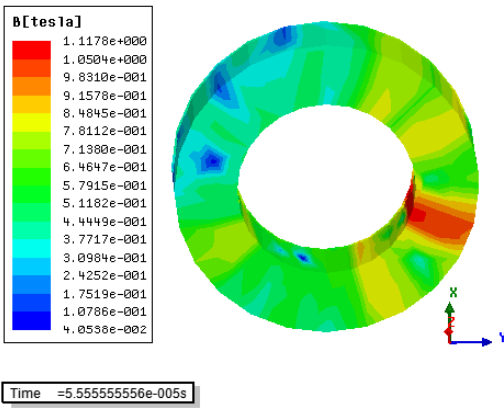

Fig. 3. Magnetic field illustration for Metglas alloy 2605SA1-based high-frequency magnetic-link in the ANSOFT (transient magnetic fields).

IV. EXPERIMENTAL VERIFICATION

To verify the feasibility of design optimization process, two prototype magnetic-links were constructed, as shown in Fig. 4, with 20 μm thick Metglas stripes of 2605S3A and 2605SA1, respectively. The Metglas sheet was glued with Araldite on the surface of each layer, providing both the electrical insulation and mechanical bonding. To minimize the proximity effect, Litz wires are used for windings with single layer placement. The prototypes were experimentally tested and results were compared. The magnetic-links are excited by a high-frequency square wave primary voltage, which is generated by a Semikron compact insulated gate bipolar transistor (IGBT) module SK30GH123 (can be operated up to 20 kHz) based full-bridge inverter supplied by a dc voltage source. An Agilent Technologies oscilloscope DS06034A with high voltage differential probe P5200 and Tektronix current probe TCPA300 was used to observe the voltage and current waveforms. The total loss (core loss plus copper loss) was measured by a universal power analyzer Voltech PW3000A. Fig. 5 shows a photograph of the experimental setup.
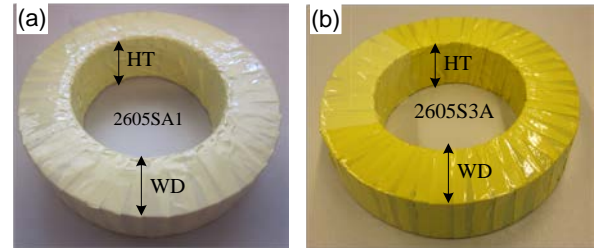

Fig. 4. Photographs of the developed cores of the prototype magnetic-links using Metglas alloys: (a) 2605SA1 and (b) 2605S3A.
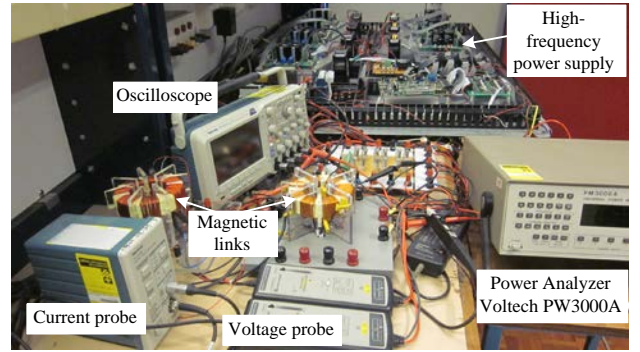

Fig. 5. A photograph of the test platform.

At 20 ^{o}C, the resistivity of copper is 1.678×10^{-8} Ωm. The total primary and secondary winding wire lengths were 2.24 m and 3.62 m, respectively. The diameters of primary and secondary winding copper wires were the same (0.4 mm), and also the cross sectional areas (12.56×10^{-8} m^2). Therefore, at the room temperature of 23 ^{o}C (during the test) 0.0233 Ω and 0.1620 Ω resistances were considered theoretically for the primary and secondary windings, respectively. The Wheatstone bridge was used to measure the winding dc resistances. The primary and secondary winding dc resistances were obtained as 0.0235 Ω and 0.1630 Ω, and they were found highly consistent with the theoretical values. The voltage transformation ratios were measured and found highly consistent with theoretical value of 1.781 with a variation of less than ± 0.08%. This is obligatory for the proposed converter.

Fig. 6 shows the *B-H* loops under a square voltage

excitation at 6 kHz. The magnetic flux density, *B*, was calculated from the measured winding voltage by Faraday's law as

$$B = \frac{1}{N_2 A_e} \int V_L dt \ . \tag{7}$$

where N_2 is number of turns in the pick-up coil and A_e the cross sectional area of the core, and V_L the pick-up coil voltage. The field intensity, *H*, was calculated from the measured current by Ampere's law as

$$H = \frac{N_1 i(t)}{l_e} \ . \tag{8}$$

where N_1 is the number of turns in the primary coil, *i(t)* the excitation current, and l_e the mean length of the core. As shown, the *B-H* loop of alloy 2605S3A is slightly narrower, i.e. lower core loss, than that of alloy 2605SA1. The maximum flux density was also calculated at different temperatures ranging from 40 °C to 120 °C to check the temperature dependency, and was found approximately constant for this temperature range. Fig. 7 shows the specific core losses against flux density measured at 6 kHz. The total power loss (core loss plus copper loss) was also measured to check the core loss calculation. As demonstrated by the results, although the prototypes made of alloys 2605SA1 and 2605S3A have almost the same volume and weight, the core loss of the one made of alloy 2605S3A is much lower than that made of alloy 2605SA1 under the same operating conditions.
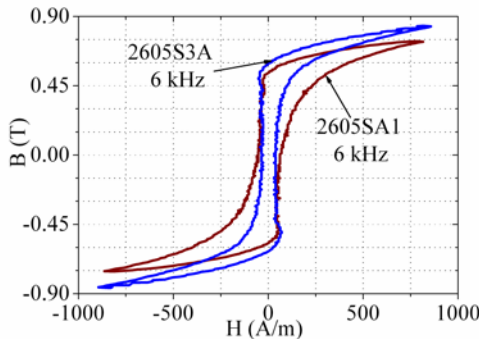

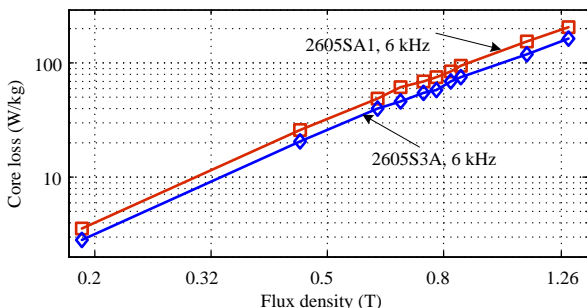Fig. 6. Measured *B-H* loops of Metglas alloys 2605S3A and 2605SA1.

Fig. 7. Measured core losses of Metglas alloys of 2605S3A and 2605SA1.

V. CONCLUSION

A method is proposed to optimize the design of amorphous alloys-based high-frequency magnetic-links for grid connected medium-voltage converters. The proposed method has been validated by a scaled down 2.5 kVA prototype system with Metglas amorphous alloys 2605S3A and 2605SA1. Experimental results are found highly consistent with the theoretical values. The same concept can be used to develop the high-power magnetic-links with other advanced magnetic materials, e.g. nanocrystalline. It is expected that the proposed new technology will have great potential for future renewable power generation systems and smart grid applications.

REFERENCES

[1] J. Mei, B. Xiao, K. Shen, L. M. Tolbert, and J. Y. Zheng, "Modular multilevel inverter with new modulation method and its application to photovoltaic grid-connected generator," *IEEE Trans. Power Electron.*, vol. 28, no. 11, pp. 5063–5073, Nov. 2013.

[2] X. Yuan, J. Chai, and Y. Li, "A transformer-less high-power converter for large permanent magnet wind generator systems," *IEEE Trans. Sust. Energy,* vol. 3, no. 3, pp.318–329, Jul. 2012.

[3] M. R. Islam, Y. G. Guo, and J. G. Zhu, "A medium-frequency transformer with multiple secondary windings for medium-voltage converter based wind turbine generating systems," *J. App. Phys.*, vol. 113, no. 17, pp. 17A324–17A324-3, May 2013.

[4] C. H. Hsu, C. Y. Lee, Y. H. Chang, F. J. Lin, C. M. Fu, and J. G. Lin, "Effect of magnetostriction on the core loss, noise, and vibration of fluxgate sensor composed of amorphous materials," *IEEE Trans. Magn.,* vol. 49, no. 7, pp. 3862–3865, Jul. 2013.

[5] A. Chrobak, A. Kaleta, P. Kwapulinski, M. kubisztal, and G. Haneczok, "Magnetic shielding effectiveness of iron-based amorphous alloy and nanocrystalline composites," *IEEE Trans. Magn.,* vol. 48, no. 4, pp. 1512–1515, Apr. 2012.

[6] M. Pasquale, C. Appino, C. P. Sasso, V. Basso, C. Beatrice, and G. Bertotti, "Analysis of stress-dependent hysteresis in soft amorphous materials," *IEEE Trans. Magn.,* vol. 37, no. 4, pp. 2281–2283, Jul. 2001.

[7] A. Makino, "Nanocrystalline soft magnetic Fe-Si-P-Cu alloy with high B of 1.8–1.9 T contributable to energy saving," *IEEE Trans. Magn.,* vol. 48, no. 4, pp. 1331–1335, Apr. 2012.

[8] M. Rada, S. Kardelky, I. Mazilu, A. Kirchner, A. Gebert, O. Gutfleisch, and L. Schultz, "Corrosion behavior of polymer-bonded NdFeB-based nanocrystalline magnets," *IEEE Trans. Magn.,* vol. 40, no. 4, pp. 2864–2866, Jul. 2004.

[9] D. Azuma and R. Hasegawa, "Core loss in toroidal cores based on Fe-based amorphous Metglas 2605HB1 Alloy," *IEEE Trans. Magn.,* vol. 47, no. 10, pp. 3460–3462, Oct. 2011.

[10] M. Mouhamad, C. Elleau, F. Mazaleyrat, C. Guillaume, and B. Jarry, "Physicochemical and accelerated aging tests of Metglas 2605SA1 and Metglas 2605HB1 amorphous ribbons for power applications," *IEEE Trans. Magn.,* vol. 47, no. 10, pp. 3192–3195, Oct. 2011.

[11] M. R. Islam, Y. G. Guo, and J. G. Zhu, "A high-frequency link multilevel cascaded medium voltage converter for direct grid integration of renewable energy systems," *IEEE Trans. Power Electron.*, vol. 29, no. 8, pp. 4167–4182, Aug. 2014.

[12] R. Storn and K. Price, "Differential evolution - A simple and efficient heuristic for global optimization over continuous spaces," J. Global Optim., vol. 11, no. 4, pp. 341–359, Dec., 1997.

[13] N. Baatar, D. H. Zhang, and C. S. Koh, "An improved differential evolution algorithm adopting λ-best mutation strategy for global optimization of electromagnetic devices, "*IEEE Trans. Magn.,* vol. 49, no. 5, pp. 2097–2100, May 2013.

[14] G. Lei, K. R. Shao, Y. G. Guo, J. G. Zhu, and J. D. Lavers, "Sequential optimization method for the design of electromagnetic device," *IEEE Trans. Magn.*, vol. 44, no. 11, pp. 3217–3220, Nov., 2008.

[15] I. Villar, "Multiphysical characterization of medium-frequency power transformers," PhD dissertation, EPFL, 2010.